biomimetics

MDPI

Article

Analysis of a Regression Model for Creating Surface Microgeometry after Machining Zirconia YML Used for Dental Application

Ján Duplák, Samuel Mikuláško *, Darina Dupláková, Maryna Yeromina and Rastislav Kaščák

Department of Automobile and Manufacturing Technologies, Faculty of Manufacturing Technologies, Technical University of Košice, Bayerova 1, 08001 Prešov, Slovakia
* Correspondence: samuel.mikulasko@tuke.sk

Abstract: This article focuses on research in the machining of zirconia crowns for dental implants. Its goal is to find the most suitable cutting parameters that significantly affect the final surface roughness of the crowns for dental implants. This study conducts investigations and experiments to specify the cutting parameters that achieve the optimal surface roughness of zirconia crowns for dental implants. The experiments were designed to precisely determine the cutting parameters that influence the surface roughness of zirconia crowns. The results of this study provide important insights for improving the manufacturing process of zirconia crowns with the specified most suitable cutting parameters. This research contributes to the enhancement of zirconia crown manufacturing techniques and the improvement in the quality and effectiveness of dental implants.

Keywords: biomaterials; dental implants; milling; zirconium; dental crown

Citation: Duplák, J.; Mikuláško, S.; Dupláková, D.; Yeromina, M.; Kaščák, R. Analysis of a Regression Model for Creating Surface Microgeometry after Machining Zirconia YML Used for Dental Application. *Biomimetics* **2024**, *9*, 473. https://doi.org/10.3390/biomimetics9080473

Academic Editor: Florian Ion Tiberiu Petrescu

Received: 26 June 2024
Revised: 1 August 2024
Accepted: 2 August 2024
Published: 5 August 2024

1. Introduction

For the proper execution of the analysis and subsequent construction of a regression model for the creation of surface microgeometry after machining, it is essential to consider the findings from recent research. The issue of surface roughness of dental crowns needs to be addressed from the perspective of multiple studies, primarily to improve their adaptation and bonding in the context of tooth restoration [1,2]. From the biological point of view, roughness could affect bacterial adhesion, which initiates plague accumulation and causes severe periodontitis or peri-implantitis [3,4]. It is well-known from machining theory and numerous conducted studies [5–8] that surface roughness is influenced by several factors, including cutting speed, feed rate, and depth of cut. Current research in the field of zirconia dental implant production focuses on optimizing cutting parameters to achieve the desired surface roughness, which is a critical quality attribute. Based on the previously conducted study, the surface roughness value should range between 0.15 and 0.63 µm [9]. However, for the purposes of final finishing (after subsequent polishing or grinding of the milled material) from a medical perspective, the values should be below 0.2 µm, at which point, the surface no longer affects bacterial colonization and adhesion [10]. Studies on the surface roughness of zirconia after milling have shown that cutting speed, depth of cut, and feed rate are the fundamental technological variables affecting roughness. The importance of cutting speed is emphasized in [11,12]. The first study [11] identified speed as the main factor influencing surface roughness during high-speed milling of pre-sintered zirconia in the finishing phase. The second study [12] described a significant impact of speed on surface roughness during the ultrasonic vibration-assisted grinding (UVAG) of sintered zirconia ceramic dental implants. However, these two studies presented conflicting conclusions; the first study highlights the potential for surface improvement at higher speeds, whereas the second study suggests that increased spindle speed may lead to increased surface

roughness. This discrepancy underscores the complexity of the machining process and the need for careful optimization of its parameters.

In addition to the aforementioned studies, it is necessary to highlight the current state of the zirconia milling process, one of the primary materials used in dental manufacturing [13–15]. The milling process itself is considered the predominant method for producing dental prostheses [16–19]. However, it is important to emphasize that research has confirmed that not only cutting conditions but also the milling strategies and their combinations can influence the final product. The type of machine used has minimal, if any, impact on the quality of the machined surface [20]. Jing et al. conducted a study comparing self-glazed zirconia machined by CNC milling and produced by additive manufacturing. Their research demonstrated this through the higher fracture strength in zirconia produced by additive manufacturing, attributed to the smaller grain size and fewer voids [21]. Residual stresses were also analyzed in conventional milling and green milling. The results suggest the possibility of eliminating surface voids but not internal ones [22]. Similarly, Chopra et al. [23] emphasized the need to study the relationship between the chemical and physical properties of zirconia oxide concerning its mechanical performance, including the impact of milling. Prescribed surface roughness characteristics are crucial for ensuring the long life of a dental product and resistance to microbes and undesirable organisms [24]. Current research in the technology of zirconia dental product milling using CNC machines with CAD/CAM technology focuses on optimizing cutting parameters to achieve the desired final surface roughness [25–27]. Experimental studies on the milling of dental crowns with a focus on final surface roughness involve various methodologies and technologies to optimize the manufacturing process. In 2021, a comparative study was conducted on the production of temporary dental crowns using different 3D printing and milling technologies, highlighting significant differences in accuracy. The research results showed high accuracy values when using milling technology [28]. Modern technologies and strategic approaches bring a significant shift towards digital technologies. Studies compared the accuracy of milling with other manufacturing methods, such as stereolithography (SLA), and found that although the finishing phase significantly affects accuracy, the manufacturing method does not [29,30]. Based on these findings, milling remains the leading technology in dental practice, examined in relation to the final surface of the dental product. In 2014, Lei and Xie identified feed rate as a fundamental parameter influencing surface roughness, with width of cut being the second influencing parameter. Based on their research results, they proposed a linear regression model to predict surface roughness, but in the context of grinding as the final surface finishing process [31].

Previous studies discussed and described research dedicated to the machining of dental materials, such as the Ti6Al4V alloy [32] and Ti3Al2.5V alloy [33]. These studies also focused on optimizing the cutting conditions, such as in the article in [34], where green machining technology was used to optimize the parameters, including X and Y direction cutting speed (mm/min), Z direction cutting speed (mm/min), spindle speed (rpm), path interval (mm), cut-in amount (mm), and finish margin. The issue of optimizing cutting parameters n, v_f, a_e, and a_p was also addressed in [35], which utilized a polycrystalline diamond tool. In an article presented by us, a combination of materials, machining parameters, and tools used was created but has not yet been published in journals and proceedings. Given the above summary of conducted studies and research, the need for ongoing research is indicated to comprehensively understand the parameters involved in the milling process and their impact on the final surface roughness. By identifying and analyzing these parameters, it is possible to predict and control the entire machining process to achieve the desired outputs. The aim of this study is to determine suitable cutting parameters through the execution of experiments in an external laboratory setting. The result is the identification of cutting parameters that, along with the use of different types of tools, significantly affect the final surface roughness of the machined surface. Based on practical requirements, it is also necessary to identify the most suitable cutting parameters in conjunction with the most appropriate tool among the three selected types. This study expands the research

area of material machining for dental applications and provides results for improving the surfaces of dental materials while simultaneously reducing surface roughness after machining, thereby potentially minimizing the need for additional surface treatments.

2. Materials and Methods

The aim of this research is to streamline the production process of zirconia dental implants using milling technology through experiments. The experiments will focus on specifying suitable cutting parameters, as the standard production process involves manufacturing implants followed by manual polishing to achieve the desired roughness of Ra 0.2 µm. The outcome of the experiments will be specified cutting parameters that achieve the desired roughness without the need for manual polishing. This experiment was realized in accordance with the Figure 1.

Figure 1. The work methodology diagram.

For the experiment, a KATANA™ Zirconia YML (Kuraray Europe GmbH, Hattersheim am Main, Germany) disc was used. This is the most advanced, highly aesthetic zirconia with enhanced graduated translucency (smooth transition from enamel to dentin) and increased durability. The disc consists of 4 layers of zirconia material with varying concentrations of yttria and corresponding mechanical and color properties. The result is a smoothly graduated brightness and translucency effect, without visible transitions and with guaranteed high flexural strength. It is used for manufacturing dental bridges, crowns (frontal and distal sections), substructure constructions for veneering, and inlays/onlays/facets. KATANA™ YML discs can also be processed with rapid sintering (54 min) with minimal waiting times. Optimized material properties improve the final precision and reduce the risk of re-manufacturing [36].

For these experiments, a Datron D5 linear scales machine was used [37]. Several types of cutters with different coating types were also used. The material being machined was a zirconia oxide disc (Table 1). The semi-finished product had a diameter of 98 mm and a thickness of 18 mm. During the experiment, 24 dental crowns were manufactured.

Table 1. Material properties [38].

Physical Properties	
Chemical composition	ZrO_2
Volume density	6.05 g/cm^3
Porosity	0.5> %
Mechanical Properties	
Microhardness Vickers	1150 (Hv 0.5)
Young's modulus	205 GPa
Tensile strength	551 MPa
Elastic modulus	186 GPa
Flexural strength	75 MPa
Compressive strength	3000 MPa
Poisson's ratio	0.33
Fracture toughness	10 MPa.m^{½}
Shear modulus	80 GPa

The experiment was prepared based on the design of the experiment method—the full factorial experiment. The focus of this study was to find the most suitable cutting parameters for the production process of dental bridges made of zirconium oxide. The measured output parameter was surface roughness (Ra). The experiments investigated cutting speed, feed rate, and depth of cut, and various tools were used. The results in the experiments were determined using the Ra parameter. For each measurement, 3 combinations of the cutting parameters X1 cutting speed, X2 feed rate, X3 depth of cut were used (Table 2). From the table, it is evident that 3 series of measurements were performed for the same cutting parameters. The individual values were the arithmetic average of 12 measurements conducted on each sample. In each of the three experiments, a different type of tool was used in the machining process. The first tool was a double-sided carbide cutter with a 30° tip angle without coating p.24 code—00781015 [39]. The second tool was a double-sided carbide cutter with a 30° tip angle with X.CEED (AlTiN) coating p.31 code 0078015L [40]. The third tool was a double-sided carbide cutter with a 15° tip angle without coating p.26 code—0068815A [39]. The cutting parameters were designed from the product catalog of the respective tools.

Table 2. Determination of factors in the design of the experiment.

Name	**Factor**	**Unit**	**−1**	**+1**
X1	Cutting speed v_c	m/min	130	150
X2	Feed per tooth f_z	mm/z	0.05	0.07
X3	Depth of cut a_p	mm	0.1	0.2

In each experiment, the same manufacturing process conditions were used, with the only variation being the choice of tools. The experiment was prepared using the WORKNC Dental software Xpert 5-Axis, where the dental model (Figure 2) to be manufactured was designed [39]. WorkNC Dental is a specialized CAD/CAM software designed for dental milling, enabling the efficient production of highly accurate dental prostheses. The software supports the import of CAD files from various sources, including intraoral and laboratory scanners, accepting formats such as STL and PLY. Users can manually or automatically designate areas of the model for machining, with options for detailed adjustment and editing of these areas.

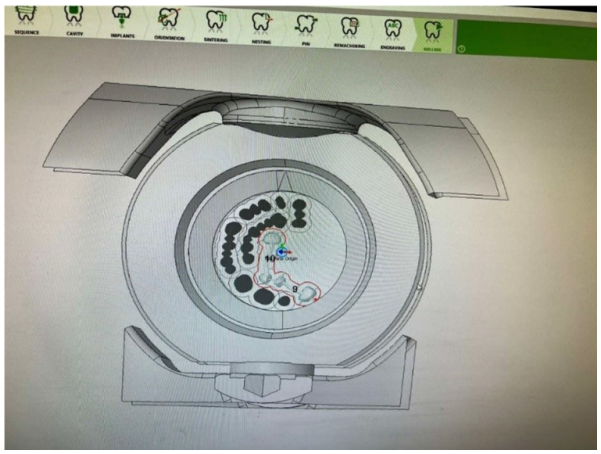

Figure 2. Model identification of the manufacturing area.

Also, then the code for CNC machining (Figure 3) on the Datron D5 machining center with a spindle characteristic of 1.8 kW; 50,000 RPM; and rotational axis tilting angles A, ±25°, and B, ±45°, was generated. WorkNC Dental allows users to define surfaces and perform calculations for the milling simulation process with high precision. Upon importing a CAD model, the software automatically identifies and analyzes the geometric properties of the model. Subsequently, the software performs the necessary calculations and generates the milling simulation process, enabling the visualization and optimization of the entire milling procedure. This process ensures that the resulting dental restorations are manufactured with the required accuracy and quality.

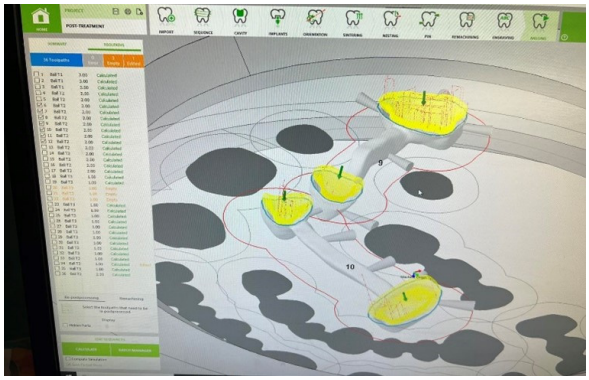

Figure 3. Defining surfaces and calculations for the milling simulation process.

This software offers a user-friendly interface that enables the milling of complex dental prostheses. It not only automates the milling process but also can be used to automate the implant placement process. It is an open-source CAM software product, meaning it can be used with any standard milling machine. Machining sequences are optimized and dependent on the material, using 4, 3 + 2, or simultaneous 5-axis strategies. The software is primarily designed for metal, ceramic, plastic, and nanocomposite materials. It features 3D machine dynamics and kinematics control. Another advantage is the automatic generation of 5-axis toolpaths for machining. With this software, machining of any type of dental component from any material is possible.

The roughness measurements were conducted in accordance with ISO 4288 (Surface texture: Profile method, 1996), utilizing a cut-off length of 0.8 mm, a measuring length of 4 mm, and a velocity of 0.1 mm/s with a Gaussian filter. Each sample had 12 measurement segments, and the surface was measured directly after machining, without any additional surface treatments.

3. Results and Discussion

3.1. Evaluation of the First Experiment

The result of the experiment is the parameter of roughness Ra. From Table 3, it is evident that three series of measurements were conducted for the same cutting parameters. The individual values are the arithmetic average of 12 measurements (12 repetitions) performed on each sample. In the first series of measurements, a tool with a 30° tip angle without coating was used in production. In the series of measurements, the cutting speeds were 130 m/min and 150 m/min, the feed per tooth was 0.05 mm/z and 0.07 mm/z, and the depth of cut was 0.1 mm and 0.2 mm.

Table 3. The first experiment—process parameters and measured value.

	v_c	f_z	a_p	**Ra**
1	130	0.05	0.1	0.22
2	130	0.05	0.2	0.31
3	130	0.07	0.1	0.26
4	130	0.07	0.2	0.21
5	150	0.05	0.1	0.18
6	150	0.05	0.2	0.13
7	150	0.07	0.1	0.24
8	150	0.07	0.2	0.30
9	130	0.05	0.1	0.28
10	130	0.05	0.2	0.41
11	130	0.07	0.1	0.33
12	130	0.07	0.2	0.47
13	150	0.05	0.1	0.21
14	150	0.05	0.2	0.19
15	150	0.07	0.1	0.34
16	150	0.07	0.2	0.41
17	130	0.05	0.1	0.36
18	130	0.05	0.2	0.29
19	130	0.07	0.1	0.45
20	130	0.07	0.2	0.37
21	150	0.05	0.1	0.24
22	150	0.05	0.2	0.19
23	150	0.07	0.1	0.36
24	150	0.07	0.2	0.40

In the conducted experiments, a significance level of 0.05 was established. This value, $\alpha = 0.05$, indicates an acceptance of a 5% risk of rejecting the null hypothesis when it is true. If the p-value is less than 0.05, the null hypothesis is rejected, indicating that the observed effect is statistically significant.

In the first experiment, the overall statistical significance of the model was established with a *p*-value of 0.035, indicating that at least one factor or interaction significantly affects the dependent variable Ra. The values for cutting speed and depth of cut are not statistically significant, while the value for feed per tooth is at the borderline of statistical significance. The interactions $v_c \cdot f_z$, $f_z \cdot a_p$, and $v_c \cdot f_z \cdot a_p$ are also not statistically significant. However, in the conducted experiment, the interaction $v_c \cdot a_p$ is statistically significant.

In the conducted analysis of variance, the total number of degrees of freedom (DF) is 23. These degrees of freedom are allocated between the individual components of the model and the error term. For the calculation of t-values, 14 degrees of freedom are attributed to the error component. The results of the analysis are presented in Figure 4.

Analysis of Variance

Source	DF	Adj SS	Adj MS	F-Value	P-Value
Model	9	0,130554	0,014506	2,94	0,035
Blocks	2	0,053358	0,026679	5,41	0,018
Linear	3	0,028246	0,009415	1,91	0,175
Vc	1	0,005704	0,005704	1,16	0,300
Fz	1	0,022204	0,022204	4,50	0,052
Ap	1	0,000337	0,000337	0,07	0,797
2-Way Interactions	3	0,041246	0,013749	2,79	0,079
Vc*Fz	1	0,004537	0,004537	0,92	0,354
Vc*Ap	1	0,034504	0,034504	7,00	0,019
Fz*Ap	1	0,002204	0,002204	0,45	0,515
3-Way Interactions	1	0,007704	0,007704	1,56	0,232
Vc*Fz*Ap	1	0,007704	0,007704	1,56	0,232
Error	14	0,069042	0,004932		
Total	23	0,199596			

Coded Coefficients

Term	Coef	SE Coef	T-Value
Constant	0,2979	0,0143	20,78
Blocks			
1	-0,0667	0,0203	-3,29
2	0,0321	0,0203	1,58
Vc	-0,0154	0,0143	-1,08
Fz	-0,0304	0,0143	-2,12
Ap	-0,0037	0,0143	-0,26
Vc*Fz	-0,0137	0,0143	-0,96
Vc*Ap	0,0379	0,0143	2,65
Fz*Ap	0,0096	0,0143	0,67
Vc*Fz*Ap	0,0179	0,0143	1,25

Figure 4. The first experiment-analysis of variance (**left**) and T-values (**right**).

The size of the factors' impact on the resulting value can be observed from the Pareto chart (Figure 5). The effects are ranked from the largest to the smallest. From the Pareto analysis conducted for the first experiment, it can be concluded that the most significant factor influencing the resulting roughness is the cutting speed in combination with the depth of cut. In this experiment, the feed rate also significantly affects the resulting surface roughness. The depth of cut alone has the least effect on the final surface roughness.

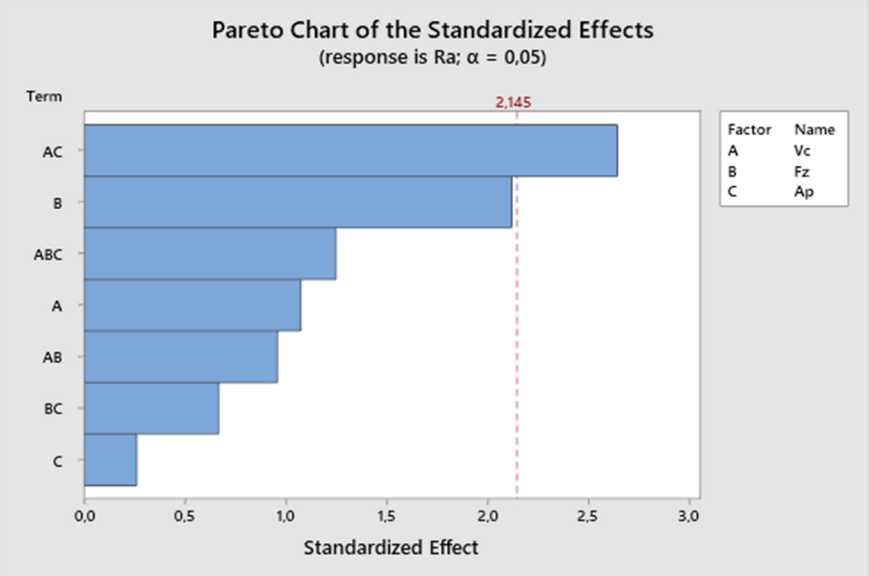

Figure 5. The first experiment—Pareto chart of the standardized effect.

From the residual plot (Figure 6), it can be seen that it is a model fulfilling the assumptions because the residual deviations are randomly distributed around zero, and the studentized residuals range from −0.2 to 0.2. The residuals do not exhibit heteroscedasticity (they form an irregular cluster), indicating no variance in the values during measurement.

The residuals align around the ideal line, indicating a normal distribution. The normal probability plot of residuals displayed in Figure 7 allows us to accept the hypothesis of residual normality.

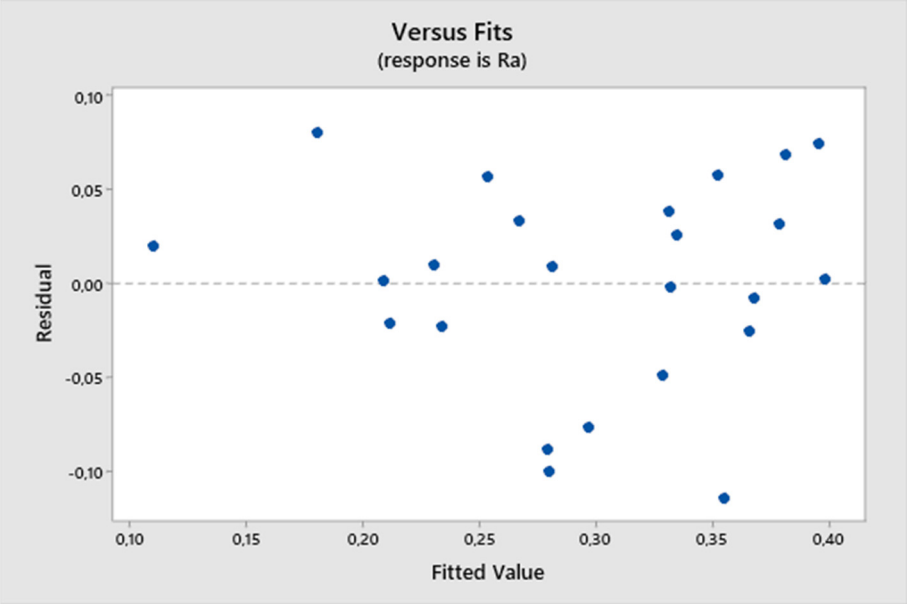

Figure 6. The first experiment-fitted values and residuals.

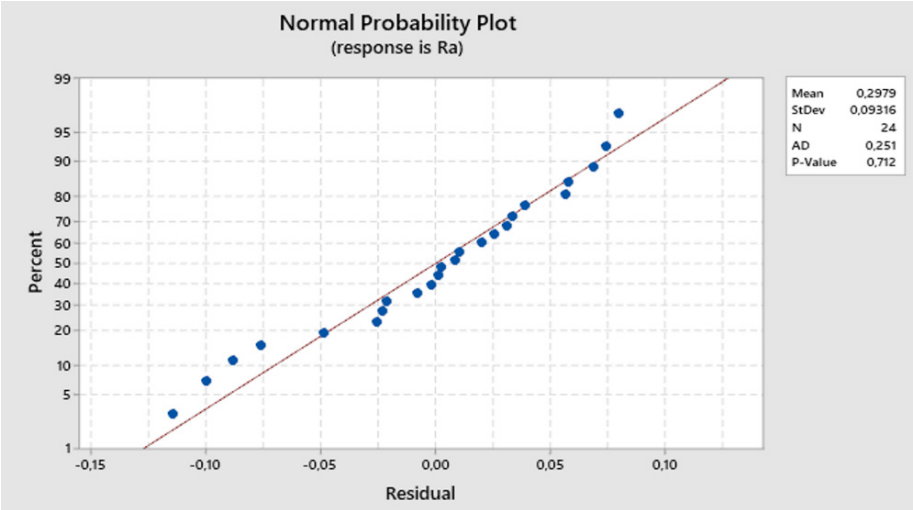

Figure 7. The first experiment-expected values and residuals.

After analyzing the variations in measurements, a regression equation was obtained. This equation denotes the surface roughness as a function of the independent factors of cutting speed, feed rate, and depth of cut. The following equation describes the basic regression model:

$$Ra = -1.43 + 0.0141v_c + 88.6f_z + 8.6a_p - 0.675v_c \cdot f_z - 0.068v_c \cdot a_p - 483f_z \cdot a_p + 3.58v_c \cdot f_z \cdot a_p \quad (1)$$

The next graph in Figure 8 describes the influence of individual parameters on the resulting surface roughness. From the graph, it can be observed that the feed rate parameter has the greatest impact on the resulting roughness, followed by the cutting speed parameter. The influence of the depth of cut parameter is much smaller in this experiment compared to others.

Figure 9 presents the reported coefficients of determination for the first experiment. The results obtained from the analysis show a coefficient of determination (R-squared) of 65.41%, which falls within the interval < 50, 80), indicating a high degree of fit. Thus, over 65% of the variability in the dependent variable can be explained by a linear relationship with the predictors. However, after adjusting for the number of predictors, the Adjusted

R-squared value decreases significantly to 43.17%, which falls within the interval < 30, 50), indicating a moderate degree of fit.

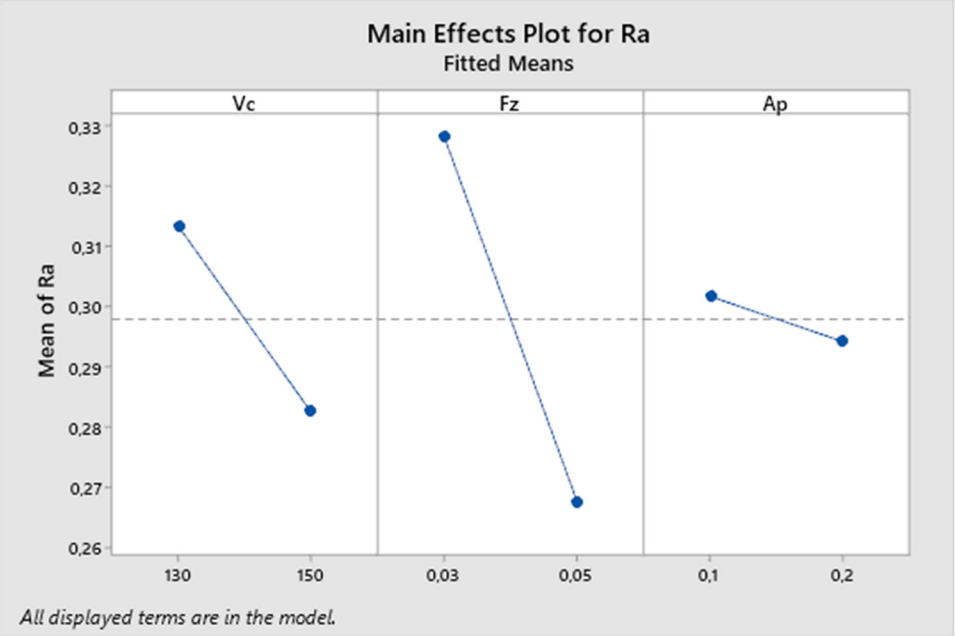

Figure 8. The first experiment-main effects plot for Ra.

Model Summary

S	R-sq	R-sq(adj)	R-sq(pred)
0,0702250	65,41%	43,17%	0,00%

Figure 9. The first experiment-model summary.

Subsequently, through backward regression, the least significant variables were gradually removed from the model to ensure the identification of only statistically significant variables. In the analyzed case, based on the reported *p*-values, the variables with the highest *p*-values were considered for removal. The first variable eliminated was the depth of cut, with a *p*-value of 0.797. Next, the interaction term $f_z \cdot a_p$ was removed, with a *p*-value of 0.515. This was followed by the elimination of $v_c \cdot f_z$ (*p*-value 0.354) and the cutting speed (*p*-value 0.300). Finally, the term $v_c \cdot f_z \cdot a_p$ was removed with a *p*-value of 0.232. The resulting regression equation includes variables with *p*-values lower than 0.05 f_z (*p*-value 0.052, which is borderline but acceptable) and $v_c \cdot a_p$ (*p*-value 0.019). The resulting regression equation after applying backward regression is as follows:

$$Ra = 0.2979 - 0.0304 f_z + 0.0379 v_c \cdot a_p \quad (2)$$

In the following graphs, the influence of different combinations of parameters on the resulting surface roughness can be observed. The most suitable surface roughness was measured on the graph $f_z \cdot v_c$, where the surface roughness was recorded at around 0.24 µm.

The following graph (Figure 10) represents the surface roughness Ra dependency on the combination of two process factors. For each measurement, the third factor is fixed at the middle level. The lowest Ra values are obtained with higher cutting speeds and higher feed rates and increase with decreasing cutting speed. The lowest Ra value is observed at v_c 150 m/min and f_z 0.05 mm/z.

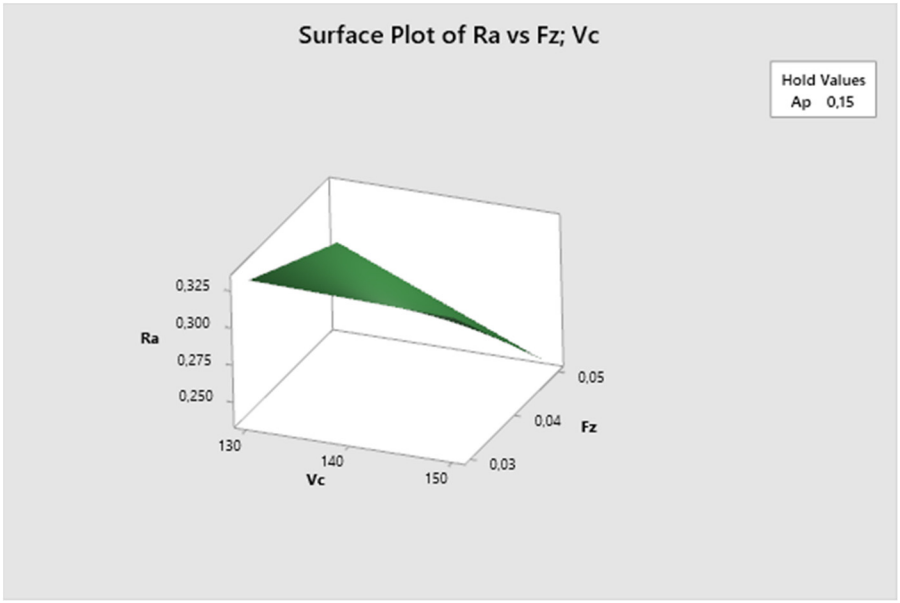

Figure 10. The first experiment-surface plot of Ra—f_z; v_c.

In this graph—Figure 11—the feed rate parameter is fixed. Here, it can be seen that the lowest Ra values are obtained with higher cutting speeds and lower depth of cut, increasing with decreasing cutting speed. The lowest Ra value is observed at v_c 150 m/min and a_p 0.1 mm.

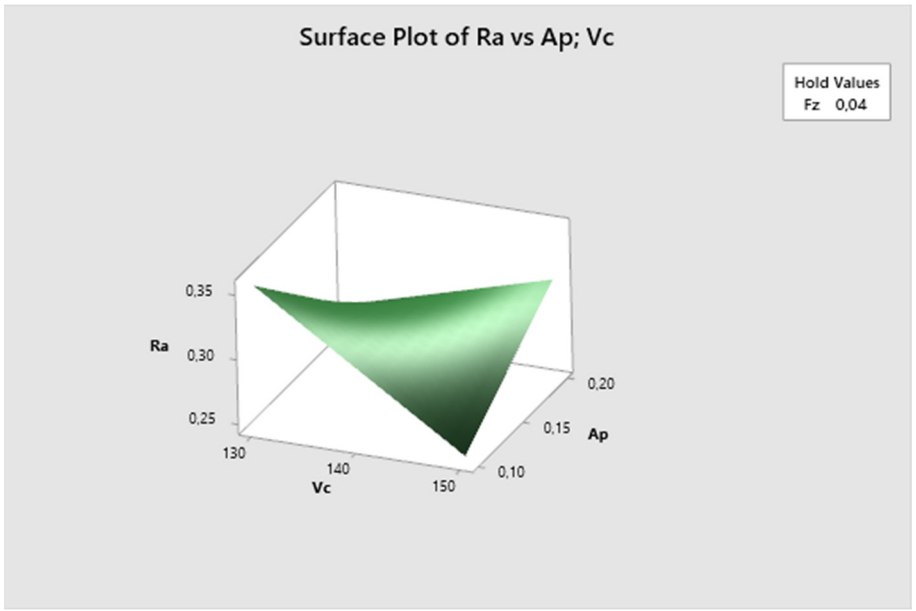

Figure 11. The first experiment-surface plot of Ra—a_p; v_c.

The cutting speed parameter is fixed in Figure 12. Here, it can be seen that the lowest Ra values are obtained with higher feed rates and lower depth of cut, increasing with higher depth of cut. The lowest Ra value is observed at f_z 0.05 mm/z and a_p 0.1 mm.

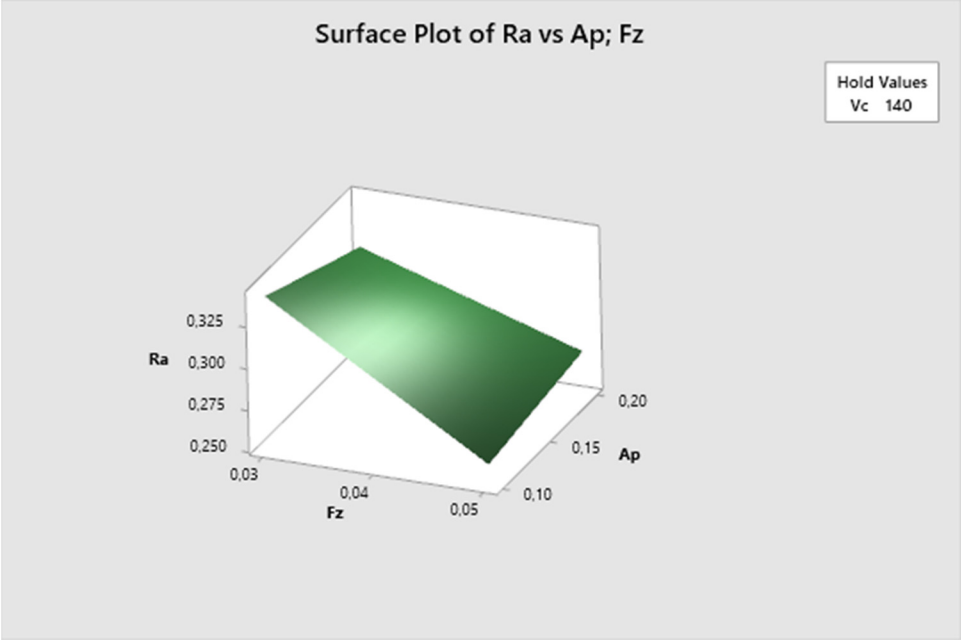

Figure 12. The first experiment-surface plot of Ra—a_p; f_z.

3.2. Evaluation of the Second Experiment

The result of the experiment is the parameter of roughness Ra. From Table 4, it is evident that three series of measurements were conducted for the same cutting parameters. The individual values are the arithmetic average of 12 measurements performed on each sample. In the first series of measurements, a tool with a 30° tip angle with coating X.CEED was used in production. In the series of measurements, the cutting speeds were 130 m/min and 150 m/min, the feed per tooth was 0.05 mm/z and 0.07 mm/z, and the depth of cut was 0.1 mm and 0.2 mm.

Table 4. The second experiment—process parameters and measured values.

	v_c	f_z	a_p	**Ra**
1	130	0.05	0.1	0.18
2	130	0.05	0.2	0.16
3	130	0.07	0.1	0.15
4	130	0.07	0.2	0.21
5	150	0.05	0.1	0.13
6	150	0.05	0.2	0.11
7	150	0.07	0.1	0.18
8	150	0.07	0.2	0.22
9	130	0.05	0.1	0.19
10	130	0.05	0.2	0.23
11	130	0.07	0.1	0.29
12	130	0.07	0.2	0.26
13	150	0.05	0.1	0.12
14	150	0.05	0.2	0.15
15	150	0.07	0.1	0.20
16	150	0.07	0.2	0.31
17	130	0.05	0.1	0.18
18	130	0.05	0.2	0.27
19	130	0.07	0.1	0.35
20	130	0.07	0.2	0.28
21	150	0.05	0.1	0.17
22	150	0.05	0.2	0.11
23	150	0.07	0.1	0.26
24	150	0.07	0.2	0.22

In the second experiment, the overall statistical significance of the model was established with a *p*-value of 0.043, indicating that at least one factor or interaction significantly influences the dependent variable Ra. The individual effects of cutting speed, depth of cut, and feed per tooth were found to be not statistically significant. Similarly, the interactions $v_c \cdot f_z$ and $f_z \cdot a_p$ were not statistically significant. However, the interactions $v_c \cdot a_p$ and $v_c \cdot f_z \cdot a_p$ were found to have a statistically significant effect.

In the conducted analysis of variance, the total number of degrees of freedom (DF) is 23. These degrees of freedom are allocated between the individual components of the model and the error term. For the calculation of t-values, 14 degrees of freedom are attributed to the error component. The results of the analysis are presented in Figure 13.

Analysis of Variance

Source	DF	Adj SS	Adj MS	F-Value	P-Value
Model	9	0,063021	0,007002	2,76	0,043
Blocks	2	0,017758	0,008879	3,49	0,059
Linear	3	0,009212	0,003071	1,21	0,343
Vc	1	0,007004	0,007004	2,76	0,119
Fz	1	0,000004	0,000004	0,00	0,968
Ap	1	0,002204	0,002204	0,87	0,367
2-Way Interactions	3	0,021546	0,007182	2,83	0,077
Vc*Fz	1	0,000504	0,000504	0,20	0,663
Vc*Ap	1	0,019837	0,019837	7,81	0,014
Fz*Ap	1	0,001204	0,001204	0,47	0,502
3-Way Interactions	1	0,014504	0,014504	5,71	0,032
Vc*Fz*Ap	1	0,014504	0,014504	5,71	0,032
Error	14	0,035575	0,002541		
Total	23	0,098596			

Coded Coefficients

Term	Coef	SE Coef	T-Value
Constant	0,2054	0,0103	19,96
Blocks			
1	-0,0379	0,0146	-2,61
2	0,0133	0,0146	0,92
Vc	-0,0171	0,0103	-1,66
Fz	-0,0004	0,0103	-0,04
Ap	0,0096	0,0103	0,93
Vc*Fz	0,0046	0,0103	-0,45
Vc*Ap	0,0288	0,0103	2,79
Fz*Ap	0,0071	0,0103	0,69
Vc*Fz*Ap	0,0246	0,0103	2,39

Figure 13. The second experiment-analysis of variance (**left**) and T-values (**right**).

Based on the measured values, a Pareto analysis was conducted. The size of the influence of factors on the resulting value can be seen from the Pareto chart (Figure 14). The effects are ranked from the largest to the smallest. From the Pareto analysis conducted for the second experiment, it can be observed that the most important factor influencing the resulting roughness is the cutting speed. Also, it is evident that the combination of all three parameters significantly affects the final surface roughness. The individual parameter feed rate is negligible in this series of measurements.

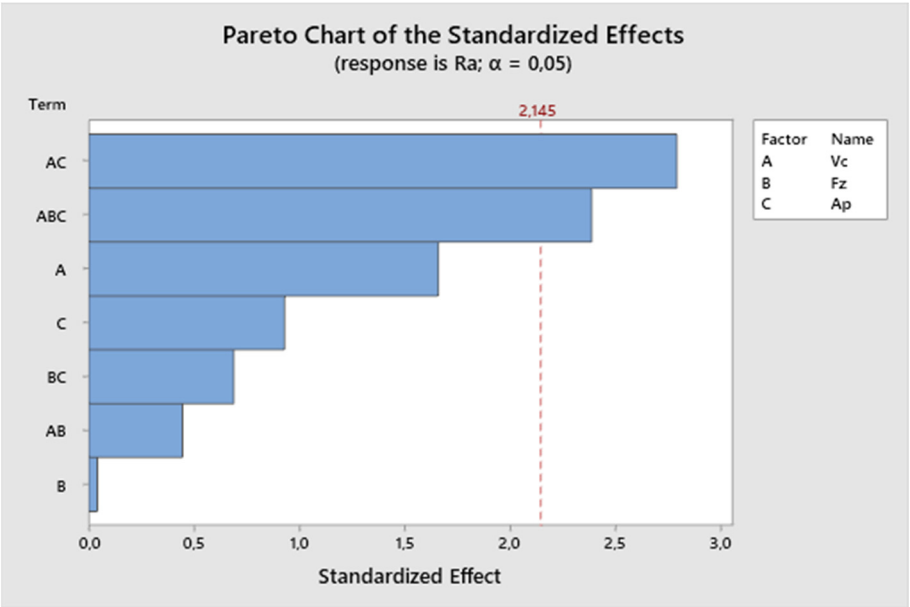

Figure 14. The second experiment-Pareto chart of the standardized effects.

From the residual plot (Figure 15), it is evident that it meets the assumptions because the residual deviations are randomly distributed around zero, and the studentized residuals range from −0.1 to 0.1. Additionally, the residuals do not exhibit heteroscedasticity (forming an irregular cluster), indicating no variance in values during the measurement.

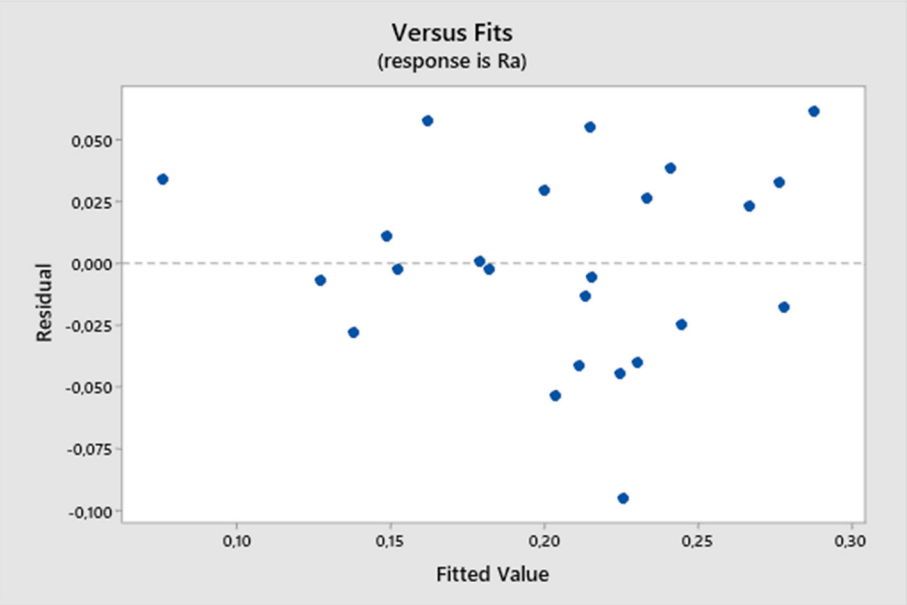

Figure 15. Second experiment-fitted values and residuals.

The residuals align around the ideal line, suggesting a normal distribution. The normal probability plot of residuals depicted in Figure 16 allows us to accept the hypothesis of normality concerning the residuals.

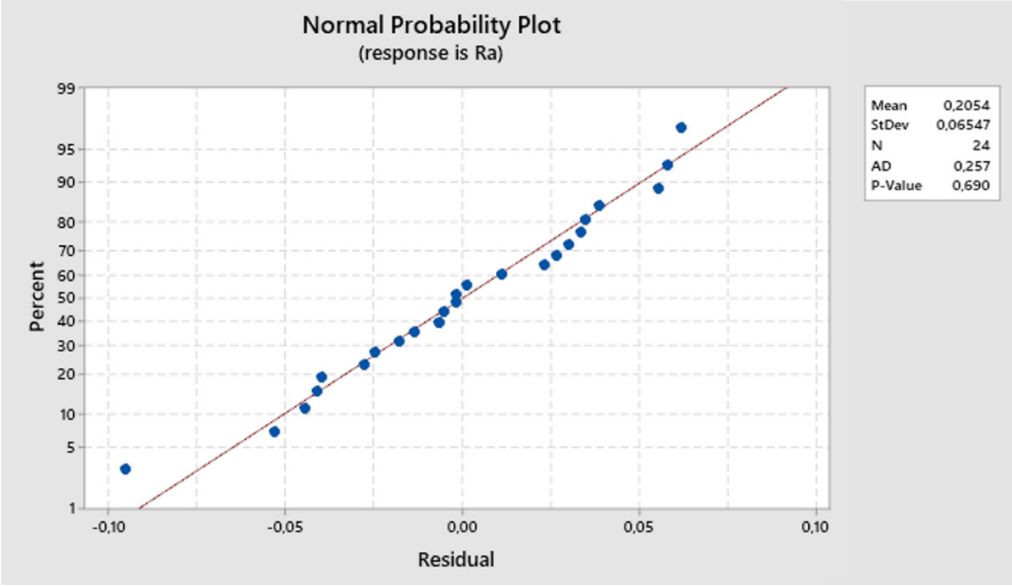

Figure 16. Second experiment-expected values and residuals.

Following the analysis of variance measurements, a regression equation was derived. This equation represents surface roughness as a function of independent factors: cutting speed, feed rate, and depth of cut. The following equation describes the basic regression model:

$$Ra = -2.68 + 0.0210v_c + 107.5F_z + 19.1a_p - 0.783v_c \cdot F_z - 0.1392v_c \cdot a_p - 674F_z \cdot a_p + 4.92v_c \cdot F_z \cdot a_p \quad (3)$$

In the next graph—Figure 17—the influence of individual parameters on the resulting surface roughness is described. From the graph, it can be noted that the cutting speed parameter has the greatest effect on the resulting roughness, followed by the depth of cut. The influence of the feed rate parameter in this experiment is much smaller compared to others.

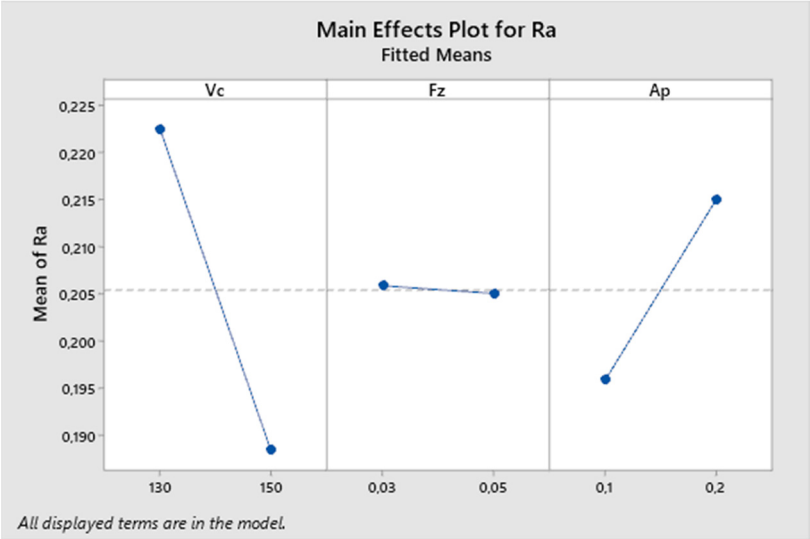

Figure 17. The second experiment-main effects plot for Ra.

Figure 18 presents the reported coefficients of determination for the second experiment. The results obtained from the analysis show a coefficient of determination (R-squared) of 63.92%, which falls within the interval < 50, 80), indicating a high degree of fit. Thus, over 65% of the variability in the dependent variable can be explained by a linear relationship with the predictors. However, after adjusting for the number of predictors, the Adjusted R-squared value decreases significantly to 40.72%, which falls within the interval < 30, 50), indicating a moderate degree of fit.

Model Summary

S	R-sq	R-sq(adj)	R-sq(pred)
0,0504090	63,92%	40,72%	0,00%

Figure 18. The second experiment-model summary.

Subsequently, through backward regression, the least significant variables were gradually removed from the model to ensure the identification of only statistically significant variables, the same as in the first experiment. In the analyzed case, based on the reported *p*-values, the variables with the highest *p*-values were considered for removal. The first variable eliminated was the feed per tooth, with a *p*-value of 0.968. Next, the interaction term $v_c \cdot f_z$ was removed, with a *p*-value of 0.663. This was followed by the elimination of $f_z \cdot a_p$ (*p*-value 0.502), the depth of cut (*p*-value 0.367), and the cutting speed (*p*-value 0.119). Finally, the resulting regression equation includes variables with *p*-values lower than 0.05: $v_c \cdot a_p$ (*p*-value 0.014) and $v_c \cdot f_z \cdot a_p$ (*p*-value 0.032). The resulting regression equation after applying backward regression is as follows:

$$Ra = 0.2054 + 0.0288v_c \cdot a_p + 0.0246v_c \cdot f_z \cdot a_p \quad (4)$$

On the following graphs, the impact of different combinations of parameters on the resulting surface roughness can be observed. The most suitable surface roughness

was observed on the $a_p \cdot v_c$ graph, where the surface roughness measured approximately 0.15 µm.

The following graph (Figure 19) illustrates the surface roughness Ra dependency on the combination of two process factors. For each measurement, the third factor is fixed at the middle level. The lowest Ra values are obtained with higher cutting speed and higher feed rate, and they increase with decreasing cutting speed. The lowest Ra value is observed at v_c 150 m/min and f_z 0.05 mm/z.

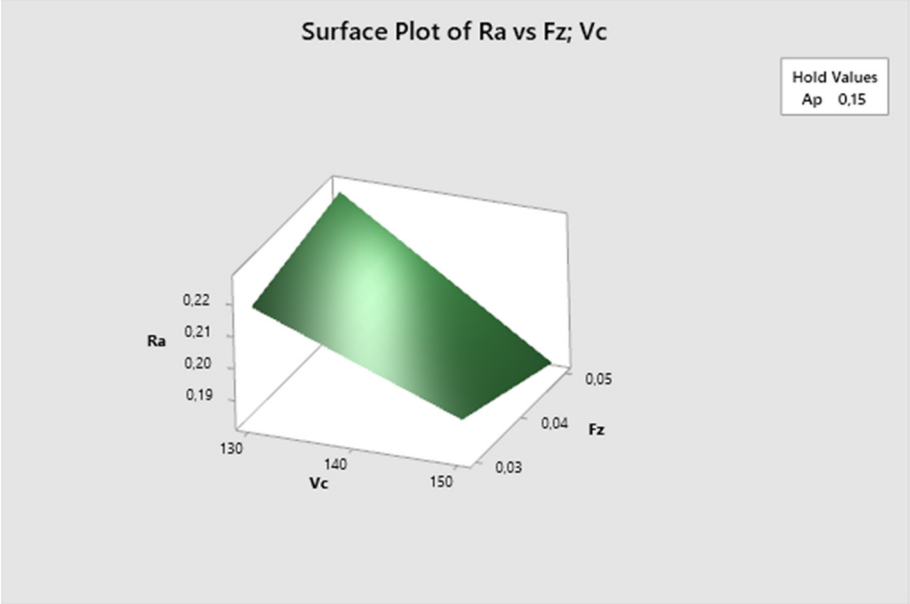

Figure 19. The second experiment-surface plot of Ra—f_z; v_c.

Figure 20 demonstrates that the feed rate parameter is fixed, and it is evident that the lowest Ra values are achieved with higher cutting speed and lower depth of cut, increasing with decreasing cutting speed. The lowest Ra value is observed at v_c 150 m/min and a_p 0.1 mm.

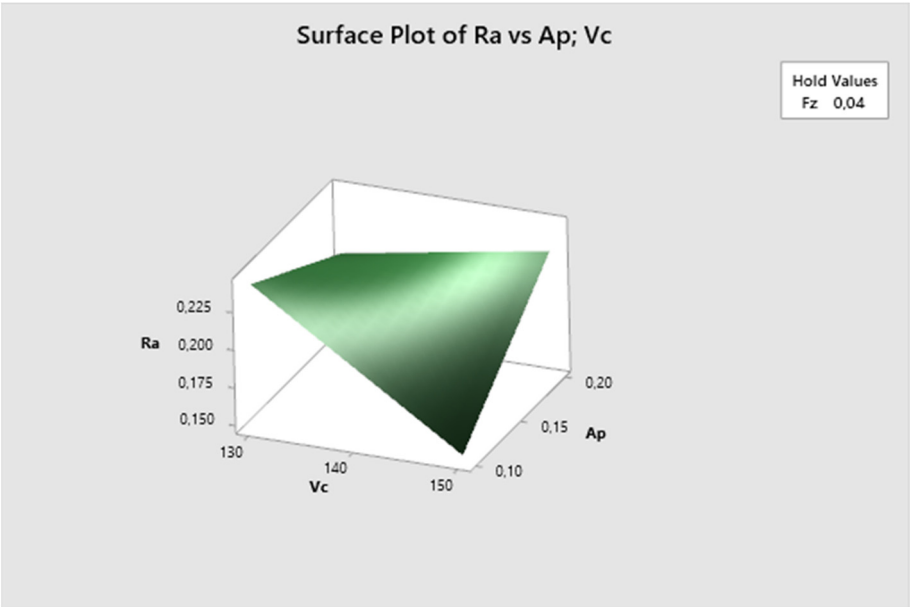

Figure 20. The second experiment-surface plot of Ra—a_p; v_c.

The cutting speed parameter is fixed in Figure 21. It is evident that the lowest Ra values are achieved with higher feed rate and lower depth of cut, increasing with higher depth of cut. The lowest Ra value is observed at f_z 0.05 mm/z and a_p 0.1 mm.

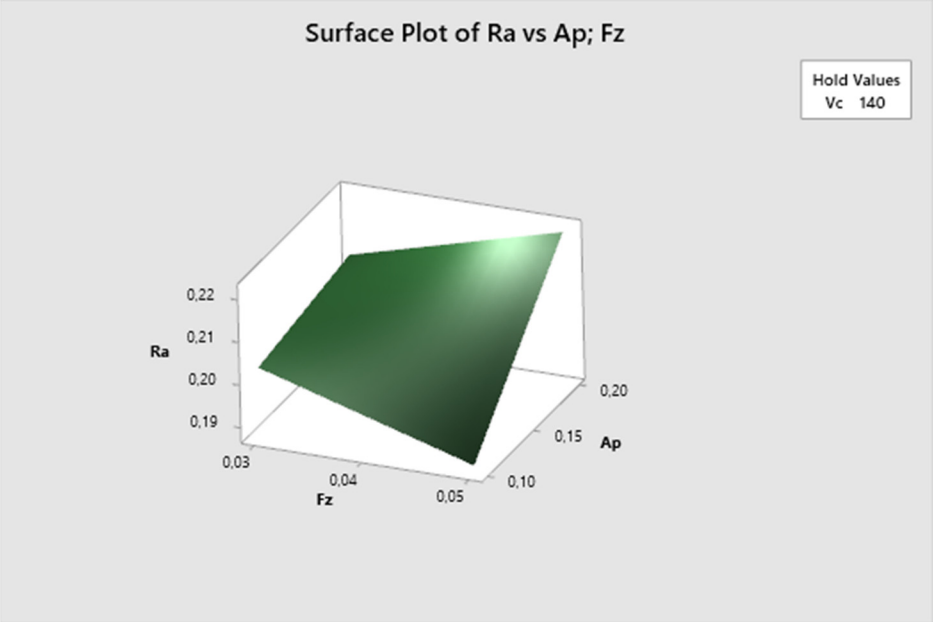

Figure 21. The second experiment-surface plot of Ra—a_p; f_z.

3.3. Evaluation of the Third Experiment

The result of the experiment is the parameter of roughness Ra. From Table 5, it is evident that three series of measurements were conducted for the same cutting parameters. The individual values are the arithmetic average of 12 measurements performed on each sample. In the first series of measurements, a tool with a 15° tip angle without coating was used in production. In the series of measurements, the cutting speeds were 130 m/min and 150 m/min, the feed per tooth was 0.05 mm/z and 0.07 mm/z, and the depth of cut was 0.1 mm and 0.2 mm.

In the third experiment, the overall statistical significance of the model is indicated by a *p*-value of 0.034, suggesting that at least one factor or interaction significantly affects the dependent variable Ra. The variables cutting speed and feed per tooth are not statistically significant. The interaction term vc×ap is also not statistically significant, while the interactions $v_c \cdot f_z$ and $v_c \cdot f_z \cdot a_p$ are on the border of statistical significance. In this experiment, the depth of cut is statistically significant, as is the interaction $f_z \cdot a_p$.

In the conducted analysis of variance, the total number of degrees of freedom (DF) is 23. These degrees of freedom are allocated between the individual components of the model and the error term. For the calculation of t-values, 14 degrees of freedom are attributed to the error component. The results of the analysis are presented in Figure 22.

The magnitude of the factors' influence on the outcome can be observed from the Pareto chart (Figure 23). The effects are ranked from largest to smallest. From the Pareto analysis conducted for the third experiment, it can be concluded that the most significant factor affecting the surface roughness is the depth of cut, combined with the feed rate this time. In this experiment, the cutting speed has much less impact on the surface roughness compared to previous experiments.

From the residual plot (Figure 24), it is evident that the model meets the assumptions because the residual deviations are randomly distributed around zero, and the studentized residuals range from −0.2 to 0.2. The residuals do not exhibit heteroscedasticity, indicating that there was no dispersion of values during the measurement.

Table 5. The third experiment—process parameters and measured values.

	v_c	f_z	a_p	Ra
1	130	0.05	0.1	0.22
2	130	0.05	0.2	0.31
3	130	0.07	0.1	0.42
4	130	0.07	0.2	0.50
5	150	0.05	0.1	0.36
6	150	0.05	0.2	0.24
7	150	0.07	0.1	0.37
8	150	0.07	0.2	0.56
9	130	0.05	0.1	0.38
10	130	0.05	0.2	0.37
11	130	0.07	0.1	0.41
12	130	0.07	0.2	0.47
13	150	0.05	0.1	0.34
14	150	0.05	0.2	0.28
15	150	0.07	0.1	0.39
16	150	0.07	0.2	0.45
17	130	0.05	0.1	0.44
18	130	0.05	0.2	0.36
19	130	0.07	0.1	0.24
20	130	0.07	0.2	0.56
21	150	0.05	0.1	0.47
22	150	0.05	0.2	0.39
23	150	0.07	0.1	0.34
24	150	0.07	0.2	0.42

Analysis of Variance

Source	DF	Adj SS	Adj MS	F-Value	P-Value
Model	9	0,125104	0,013900	2,96	0,034
Blocks	2	0,003608	0,001804	0,38	0,688
Linear	3	0,050979	0,016993	3,62	0,040
Vc	1	0,000504	0,000504	0,11	0,748
Fz	1	0,004538	0,004538	0,97	0,342
Ap	1	0,045938	0,045938	9,78	0,007
2-Way Interactions	3	0,051812	0,017271	3,68	0,038
Vc*Fz	1	0,017604	0,017604	3,75	0,073
Vc*Ap	1	0,001204	0,001204	0,26	0,621
Fz*Ap	1	0,033004	0,033004	7,02	0,019
3-Way Interactions	1	0,018704	0,018704	3,98	0,066
Vc*Fz*Ap	1	0,018704	0,018704	3,98	0,066
Error	14	0,065792	0,004699		
Total	23	0,190896			

Coded Coefficients

Term	Coef	SE Coef	T-Value
Constant	0,3871	0,0140	27,66
Blocks			
1	0,0154	0,0198	0,78
2	-0,0008	0,0198	-0,04
Vc	0,0046	0,0140	0,33
Fz	0,0138	0,0140	0,98
Ap	0,0438	0,0140	3,13
Vc*Fz	-0,0271	0,0140	-1,94
Vc*Ap	-0,0071	0,0140	-0,51
Fz*Ap	0,0371	0,0140	2,65
Vc*Fz*Ap	0,0279	0,0140	2,00

Figure 22. The third experiment—analysis of variance (**left**) and T-values (**right**).

The residuals align around the ideal line, suggesting that they follow a normal distribution. The normal probability plot of residuals, shown in Figure 25, supports accepting the hypothesis of residual normality.

After analyzing the variations in measurements, a regression equation was derived. This equation represents surface roughness as a function of independent factors: cutting speed, feed rate, and depth of cut. The following equation describes the basic regression model:

$$Ra = -5.92 + 0.0469v_c + 145.4f_z + 31.2a_p - 1.108v_c \cdot f_z - 0.2372v_c \cdot a_p - 707f_z \cdot a_p + 5.58v_c \cdot f_z \cdot a_p \quad (5)$$

In the next graph in Figure 26, the influence of each parameter on the resulting surface roughness is described. From the graph, it is evident that the parameter with the greatest impact on surface roughness is the depth of cut. The influence of the cutting speed and feed rate parameters is much smaller in this experiment compared to others.

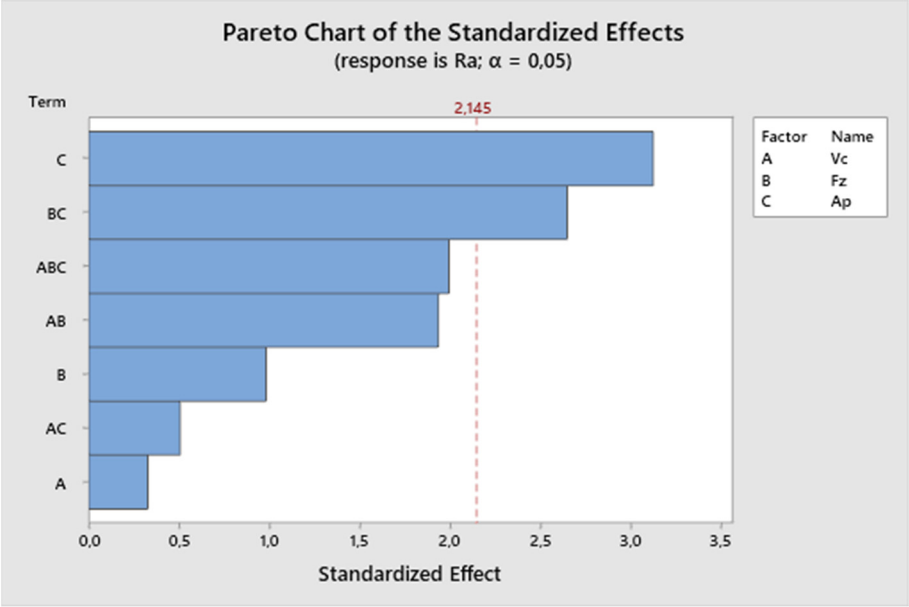

Figure 23. The third experiment-Pareto chart of the standardized effect.

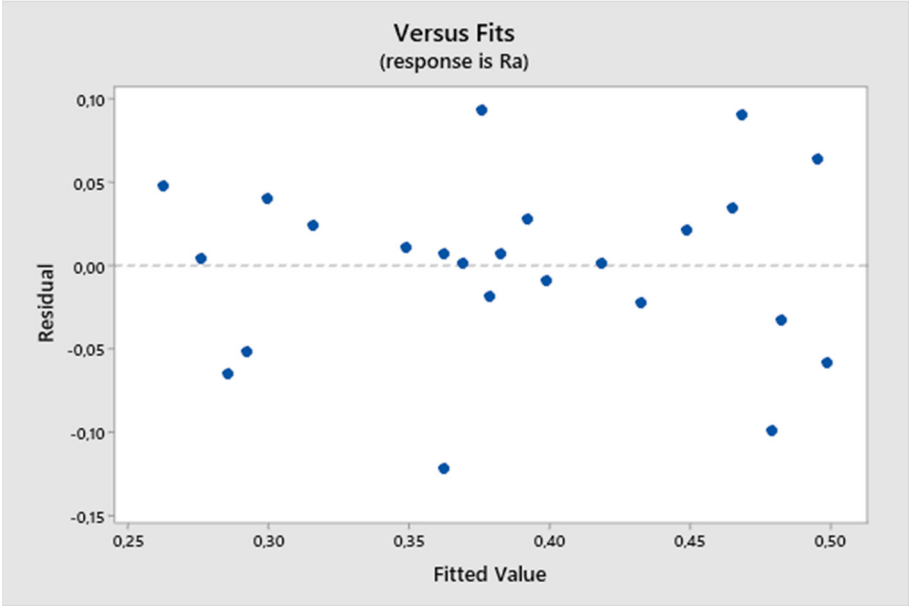

Figure 24. The third experiment-fitted values and residuals.

Figure 27 presents the reported coefficients of determination for the third experiment. The results obtained from the analysis show a coefficient of determination (R-squared) of 65.54%, which falls within the interval < 50, 80), indicating a high degree of fit. Thus, over 65% of the variability in the dependent variable can be explained by a linear relationship with the predictors. However, after adjusting for the number of predictors, the Adjusted R-squared value decreases significantly to 43.38%, which falls within the interval < 30, 50), indicating a moderate degree of fit.

Subsequently, through backward regression, the least significant variables were gradually removed from the model to ensure the identification of only statistically significant variables, the same as in the first and the second experiments. The first variable eliminated was the velocity of cutting, with a *p*-value of 0.748. Next, the interaction term $v_c \cdot a_p$ was removed, with a *p*-value of 0.621. This was followed by the elimination of feed per tooth (*p*-value 0.342), then the interaction term $v_c \cdot f_z$ (*p*-value 0.073), and the interaction term

$v_c \cdot f_z \cdot a_p$ (p-value 0.066). Finally, the resulting regression equation includes variables with p-values lower than 0.05: depth of cut (p-value 0.007) and $f_z \cdot a_p$ (p-value 0.019). The resulting regression equation after applying backward regression is as follows:

$$Ra = 0.3871 + 0.0438a_p + 0.0371f_z \cdot a_p \quad (6)$$

In the subsequent graphs, one can observe the impact of different combinations of parameters on the resulting surface roughness. The most suitable surface roughness was measured on the $a_p \cdot f_z$ graph, where the surface roughness was approximately 0.33 µm.

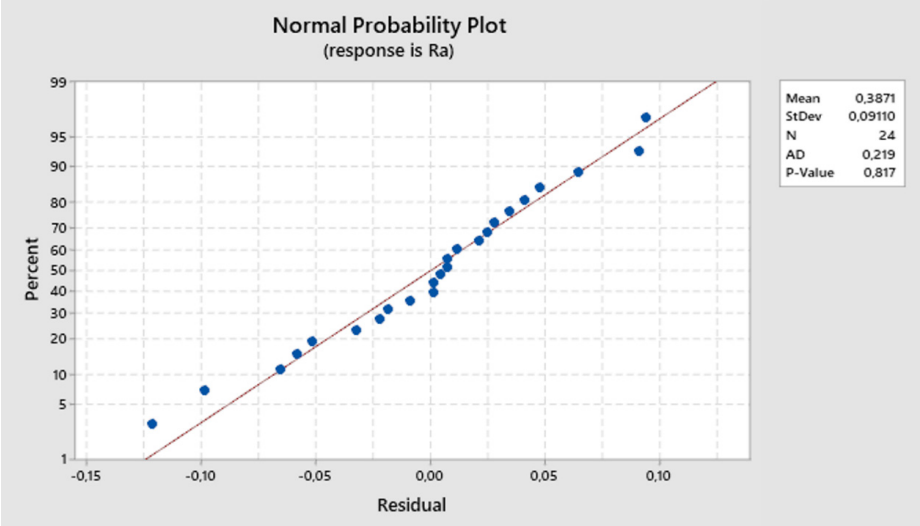

Figure 25. The third experiment-expected values and residuals.

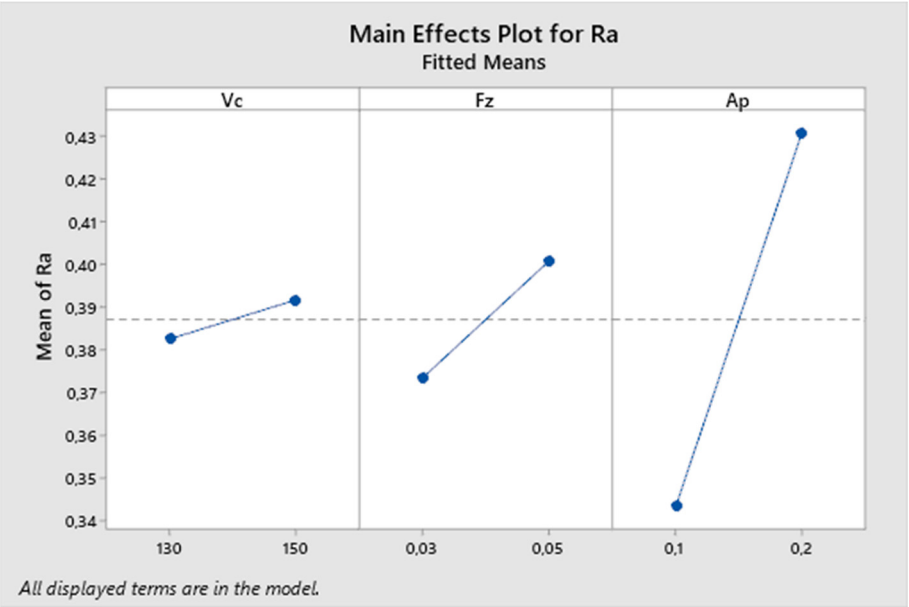

Figure 26. The third experiment-main effects plot for Ra.

Model Summary

S	R-sq	R-sq(adj)	R-sq(pred)
0,0685522	65,54%	43,38%	0,00%

Figure 27. The third experiment-model summary.

The following graph (Figure 28) illustrates the surface roughness Ra dependency on the combination of two process factors. For each measurement, the third factor is fixed at the middle level. The lowest Ra values are obtained with lower cutting speed and lower feed per tooth, and they increase with decreasing cutting speed. The lowest Ra value is observed at v_c 130 m/min and f_z 0.03 mm/z.

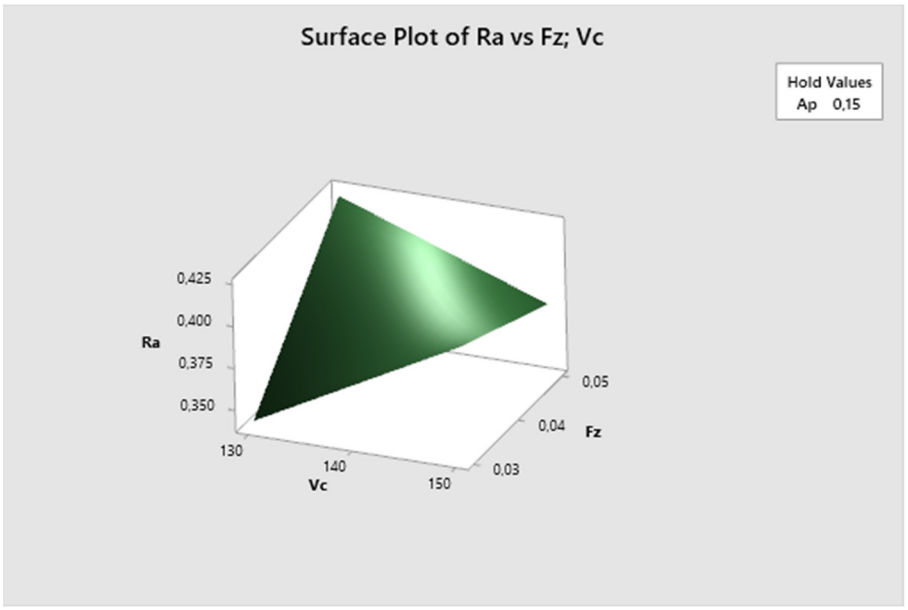

Figure 28. The third experiment-surface plot of Ra—f_z; v_c.

The feed per tooth parameter is fixed in Figure 29, and it is evident that the lowest Ra values are achieved with lower cutting speed and shallower depth of cut, increasing with decreasing cutting speed. The lowest Ra value is observed at v_c 130 m/min and a_p 0.1 mm.

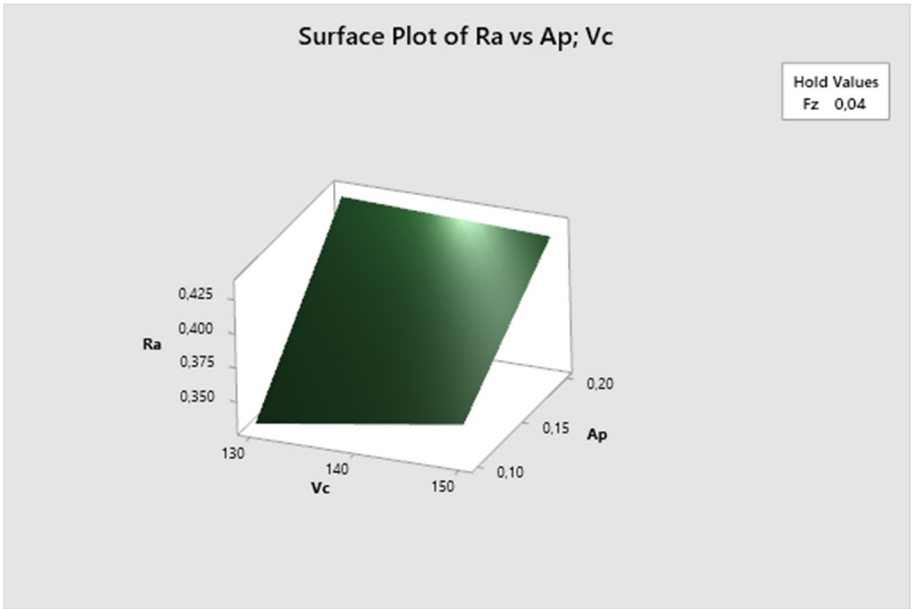

Figure 29. The third experiment-surface plot of Ra—a_p; v_c.

Figure 30 displays that the cutting speed parameter is fixed. It is evident that the lowest Ra values are obtained with higher feed per tooth and shallower depth of cut,

increasing with the higher depth of cut. The lowest Ra value is observed at f_z 0.05 mm/z and a_p 0.1 mm.

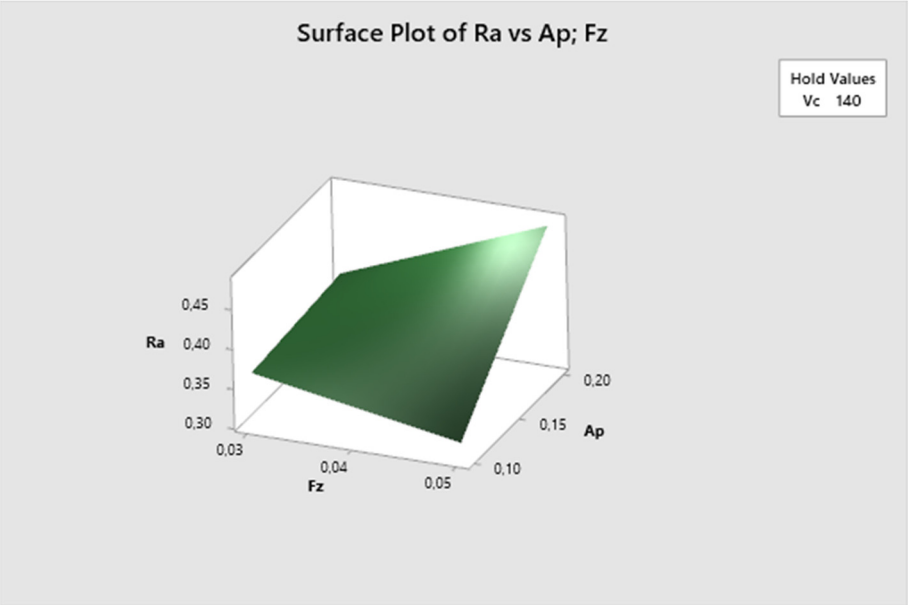

Figure 30. The third experiment-surface plot of Ra—a_p; f_z.

The conducted study examined the impact of optimized cutting parameters on the efficiency of production and the quality of zirconia dental crowns. Based on the obtained results, it was found that the correct setting of cutting parameters such as cutting speed, feed per tooth, and depth of cut, in conjunction with the appropriate tool selection, leads to a significant reduction in surface roughness to below 0.2 µm, which is crucial for dental applications without the need for further surface polishing. The achieved results are consistent with previous studies [35,41–43], which also emphasize the importance of optimizing cutting parameters to achieve high surface quality. Future research should include a broader range of machining conditions and long-term monitoring of the quality and durability of zirconia crowns in clinical practice. In conclusion, our findings highlight the importance of optimizing cutting parameters to improve the quality and efficiency of zirconia dental crown production, and further research should continue to explore and refine these parameters for even better and more consistent results.

A contact profilometer was used for measuring surface roughness, operating on the principle of direct contact between the sensor and the examined surface. Surface irregularities were recorded by the movement of a stylus probe over the sample's surface. The AFM (Atomic Force Microscopy) method can also be used to characterize material surfaces [44], which records height differences as changes in the force acting on the probe tip. This method is currently primarily employed in the field of nanomeasurement, with a focus on cellular research [45], or nano-engineered implants [46].

The cutting parameters set this way in the machining of zirconia dental crowns influence manufacturing efficiency and product quality. Proper adjustment of parameters such as cutting speed, feed per tooth, and depth of cut leads to a higher quality surface finish of the crowns, reducing surface roughness (Ra) and minimizing surface defects such as microcracks. These cutting parameters also enhance manufacturing efficiency by reducing tool wear, thereby extending tool life and lowering tool replacement costs. The efficient use of cutting parameters shortens production times and increases productivity, allowing for faster production of crowns with consistently high quality. This approach achieves greater precision and reliability in the manufacturing process of zirconia dental crowns, leading to better patient outcomes and higher competitiveness for manufacturers.

The future direction of machining zirconia crowns for dental implants includes several innovations and trends aimed at improving the quality, efficiency, and accuracy of production. In the context of zirconia crown machining, the future direction could focus on highly progressive intelligent machining. This involves the use of machines with adaptive control, which automatically adjust cutting parameters based on real-time machining conditions. As a result, even lower surface roughness values (Ra) could be achieved. Another step in the future could be the use of advanced tools such as diamond tools. The use of diamond tools for machining zirconia can ensure excellent surface quality, as can tools with nanostructured coatings: nanotechnology enables the creation of coatings that increase tool wear resistance and improve the final surface roughness of the machined part.

4. Conclusions

The milling of dental materials is currently a highly prevalent technology for producing dental products. The conducted study revealed that the selection of tools and the combination of cutting parameters significantly affect the final surface roughness of dental crowns. Both coated and uncoated tools were used for machining. The results indicate that coated tools with an appropriate tip angle substantially influence the final surface roughness, which greatly impacts the efficiency of manufacturing dental implant crowns. In the first series, an uncoated tool with a 30° tip angle was used. This experiment yielded higher Ra values, which are not very suitable for patients as additional operations, such as final surface polishing, are necessary due to the surface roughness results. In the second series, a tool with a 30° tip angle and X.CEED (AlTiN) coating was used. This experiment achieved the lowest Ra values, which are very suitable for patients since, with parameters v_c 150, f_z 0.05, and a_p 0.1/0.2, all measurements resulted in surface roughness values below 0.2 µm. In the final series, a tool with a 15° tip angle was used, achieving values between 0.22 and 0.56 µm. Based on the conducted study, it can be indicated that the most suitable tool for the specified machining parameters of YML zirconia is a coated tool with an X.CEED (AlTiN) coating and a 30° tip angle. Considering the requirements of this practice, the second series of experiments is the most suitable.

Author Contributions: Conceptualization, J.D., S.M. and D.D.; methodology, J.D., S.M. and R.K.; software, M.Y.; validation, J.D. and D.D.; formal analysis, J.D. and D.D.; investigation, J.D., S.M., D.D., M.Y. and R.K.; writing—original draft preparation, S.M., D.D. and M.Y. All authors have read and agreed to the published version of the manuscript.

Funding: This research was supported by the Scientific Grant Agency Ministry of Education, Science, Research and Sport of the Slovak Republic and Slovak Academy of Sciences, grant no. VEGA 1/0258/24, and by the Cultural and Educational Grant Agency Ministry of Education, Science, Research and Sport of the Slovak Republic, grant no. 024TUKE-4/2023. This work was supported by the Slovak Research and Development Agency under contract No. APVV-21-0293.

Institutional Review Board Statement: Not applicable.

Data Availability Statement: The original contributions presented in the study are included in the article material, further inquiries can be directed to the corresponding author.

Conflicts of Interest: The authors declare no conflicts of interest.

References

1. Lee, J.; Saleah, S.A.; Jeon, B.; Wijesinghe, R.E.; Lee, D.E.; Jeon, M.; Kim, J. Assessment of the inner surface roughness of 3D printed dental crowns via optical coherence tomography using a roughness quantification algorithm. *IEEE Access* **2020**, *8*, 133854–133864. [CrossRef]
2. Kłonica, M.; Matuszak, J.; Zagórski, I. Effect of milling technology on selected surface layer properties. In Proceedings of the 2019 IEEE 5th International Workshop on Metrology for AeroSpace (MetroAeroSpace), Turin, Italy, 19–21 June 2019; IEEE: Piscataway, NJ, USA, 2019; pp. 371–375.
3. Zeng, J.; Song, J.; Zhang, Y.; Yang, Z.; Nie, E.; Zhang, C.; Jiang, R. Surface roughness and bacteria adhesion of full zirconia restoration after different polishing treatment. *Chin. J. Tissue Eng. Res.* **2023**, *27*, 3320.

4. Fernandes, B.F.; Silva, N.; Da Cruz, M.B.; Garret, G.; Carvalho, Ó.; Silva, F.; Mata, A.; Francisco, H.; Marques, J.F. Cell Biological and Antibacterial Evaluation of a New Approach to Zirconia Implant Surfaces Modified with MTA. *Biomimetics* **2024**, *9*, 155. [CrossRef]
5. Denkena, B.; Breidenstein, B.; Busemann, S.; Lehr, C.M. Impact of hard machining on zirconia based ceramics for dental applications. *Procedia Cirp* **2017**, *65*, 248–252. [CrossRef]
6. Panda, A.; Nahornyi, V.; Valíček, J.; Harničárová, M.; Kušnerová, M.; Baron, P.; Pandova, I.; Soročin, P. A novel method for online monitoring of surface quality and predicting tool wear conditions in machining of materials. *Int. J. Adv. Manuf. Technol.* **2022**, *123*, 3599–3612. [CrossRef]
7. Valíček, J.; Harničárová, M.; Öchsner, A.; Hutyrová, Z.; Kušnerová, M.; Tozan, H.; Michenka, V.; Sepelak, V.; Mital, D.; Zajac, J. Quantifying the mechanical properties of materials and the process of elastic-plastic deformation under external stress on material. *Materials* **2015**, *8*, 7401–7422. [CrossRef]
8. Mascenik, J.; Coranic, T.; Kuchar, J.; Hazdra, Z. Influence of Selected Parameters of Zinc Electroplating on Surface Quality and Layer Thickness. *Coatings* **2024**, *14*, 579. [CrossRef]
9. Baysal, N.; Tuğba Kalyoncuoğlu, Ü.; Ayyıldız, S. Mechanical properties and bond strength of additively manufactured and milled dental zirconia: A pilot study. *J. Prosthodont.* **2022**, *31*, 629–634. [CrossRef]
10. Abdul Hamid, R.; Wan Muhamad, W.N.; Izamshah, R.; Kasim, M.S. Surface roughness analysis of zirconia dental restoration manufactured through cnc milling machine. In *Intelligent Manufacturing and Mechatronics: Proceedings of the 2nd Symposium on Intelligent Manufacturing and Mechatronics–SympoSIMM 2019, Melaka, Malaysia, 8 July 2019*; Springer: Singapore, 2020; pp. 361–371.
11. Liu, J.W.; Yang, X.J. Effect of milling parameters on surface roughness for high-speed milling of pre-sintering zirconia. *Adv. Mater. Res.* **2014**, *988*, 253–256. [CrossRef]
12. Dong, S.; Zheng, K.; Xiao, X.Z. Ultrasonic vibration assisted grinding of sintered dental zirconia ceramics: An experimental study on surface roughness. *Adv. Mater. Res.* **2014**, *1017*, 800–805. [CrossRef]
13. Manicone, P.F.; Iommetti, P.R.; Raffaelli, L. An overview of zirconia ceramics: Basic properties and clinical applications. *J. Dent.* **2007**, *35*, 819–826. [CrossRef] [PubMed]
14. Osman, R.B.; Swain, M.V. A critical review of dental implant materials with an emphasis on titanium versus zirconia. *Materials* **2015**, *8*, 932–958. [CrossRef]
15. Zhang, Y.; Lawn, B.R. Novel zirconia materials in dentistry. *J. Dent. Res.* **2018**, *97*, 140–147. [CrossRef]
16. Vera, V.; Corchado, E.; Redondo, R.; Sedano, J.; Garcia, A.E. Applying soft computing techniques to optimise a dental milling process. *Neurocomputing* **2013**, *109*, 94–104. [CrossRef]
17. Herpel, C.; Tasaka, A.; Higuchi, S.; Finke, D.; Kühle, R.; Odaka, K.; Rues, S.; Lux, C.; Yamashita, S.; Rammelsberg, P.; et al. Accuracy of 3D printing compared with milling—A multi-center analysis of try-in dentures. *J. Dent.* **2021**, *110*, 103681. [CrossRef] [PubMed]
18. Grande, F.; Tesini, F.; Pozzan, M.C.; Zamperoli, E.M.; Carossa, M.; Catapano, S. Comparison of the accuracy between denture bases produced by subtractive and additive manufacturing methods: A pilot study. *Prosthesis* **2022**, *4*, 151–159. [CrossRef]
19. Barraclough, O.; Gray, D.; Ali, Z.; Nattress, B. Modern partial dentures-part 1: Novel manufacturing techniques. *Br. Dent. J.* **2021**, *230*, 651–657. [CrossRef]
20. Dejkun, V.; Dietz, S.; Abele, E. Influence on surface quality in milling of green stage zirconia for dental products. *Appl. Mech. Mater.* **2015**, *794*, 201–206. [CrossRef]
21. Jing, Z.; Ke, Z.; Yihong, L.; Zhijian, S. Effect of Multistep Processing Technique on the Formation of Micro-defects and Residual Stresses in Zirconia Dental Restorations. *J. Prosthodont.* **2014**, *23*, 206–212. [CrossRef]
22. Zhang, Y.; Han, J.M.; Zheng, G.; Lin, H.; Bai, W.; Zhao, J.; Shen, Z. Fatigue behaviours of the zirconia dental restorations prepared by two manufacturing methods. *Adv. Appl. Ceram.* **2017**, *116*, 368–375. [CrossRef]
23. Chopra, D.; Guo, T.; Gulati, K.; Ivanovski, S. Load, unload and repeat: Understanding the mechanical characteristics of zirconia in dentistry. *Dent. Mater.* **2024**, *40*, e1–e17. [CrossRef]
24. Baghel, P.; Singh, S.; Nagdeve, L.; Jain, V.K.; Sharma, N.D. Preliminary investigations into finishing of artificial dental crown. *Int. J. Precis. Technol.* **2015**, *5*, 229–245. [CrossRef]
25. Lebon, N.; Tapie, L.; Vennat, E. Influence of milling tool and prosthetic materials on roughness of the dental CAD CAM prostheses in end milling mode. *Appl. Sci.* **2020**, *10*, 2238. [CrossRef]
26. Pacquet, W.; Tapie, L.; Mawussi, B.; Boitelle, P. Volumetric and dimensional accuracy assessment of CAD-CAM–manufactured dental prostheses from different materials. *J. Prosthet. Dent.* **2023**, *129*, 150–159. [CrossRef] [PubMed]
27. Nicolas, L.; Laurent, T. Surface Integrity of Pre-sintered Ceramics and Composites Used for Dental Prostheses After CAD/CAM Abrasive Milling. *Procedia CIRP* **2022**, *108*, 252–257. [CrossRef]
28. Son, K.; Lee, J.H.; Lee, K.B. Comparison of intaglio surface trueness of interim dental crowns fabricated with SLA 3D printing, DLP 3D printing, and milling technologies. *Healthcare* **2021**, *9*, 983. [CrossRef]
29. Li, R.; Chen, H.; Wang, Y.; Sun, Y. Performance of stereolithography and milling in fabricating monolithic zirconia crowns with different finish line designs. *J. Mech. Behav. Biomed. Mater.* **2021**, *115*, 104255. [CrossRef]
30. Lu, Y.; Wang, L.; Dal Piva AM, D.O.; Tribst JP, M.; Nedeljkovic, I.; Kleverlaan, C.J.; Feilzer, A.J. Influence of surface finishing and printing layer orientation on surface roughness and flexural strength of stereolithography-manufactured dental zirconia. *J. Mech. Behav. Biomed. Mater.* **2023**, *143*, 105944. [CrossRef] [PubMed]

31. Lei, X.B.; Xie, F. Surface roughness prediction and experimental analysis in grinding the material of zirconia used by dental restoration. *Mater. Sci. Forum* **2014**, *800*, 160–166. [CrossRef]
32. Roushan, A.; Rao, U.S.; Patra, K.; Sahoo, P. Multi-characteristics optimization in micro-milling of Ti6Al4V alloy. *J. Phys. Conf. Ser.* **2021**, *1950*, 012046. [CrossRef]
33. Raghavendra, M.J.; Ramachandra, C.G.; Srinivas, T.R.; Pai, M.P. Optimization of surface roughness of Titanium Gr-9 Alloy Turning using Taguchi method. *IOP Conf. Ser. Mater. Sci. Eng.* **2021**, *1013*, 012001. [CrossRef]
34. Dantas, T.A.; Pinto, P.; Vaz, P.C.; Silva, F.S. Design and optimization of zirconia functional surfaces for dental implants applications. *Ceram. Int.* **2020**, *46*, 16328–16336. [CrossRef]
35. Yan, X.; Dong, S.; Li, X.; Zhao, Z.; Dong, S. A Optimization of machining parameters for milling zirconia ceramics by polycrystalline diamond tool. *Materials* **2021**, *15*, 208. [CrossRef]
36. CAD/CAM Discs. Multi-Layered Zirconia Katana Disc by Kuraray Noritake. Available online: https://www.kuraraynoritake.eu/en/labside/zirconia (accessed on 12 June 2024).
37. DATRON D5 Linear Scale. DATRON AG. Available online: https://www.datron.de/products/dental-cad/cam/datron-d5-linear-scale (accessed on 11 June 2024).
38. Zirconium Oxide, Zirconia, ZrO2. Available online: https://www.matweb.com/search/datasheet.aspx?MatGUID=0742ddaddf80467fb6532e025c694e89&ckck=1 (accessed on 13 June 2024).
39. Catalogue of Tools DATRON. 2017. Available online: https://www.datron.sk/data/datron.sk/documents/DATRON_Katalog_nastroju-2018_CZ_V0.4_1538216052.pdf (accessed on 24 June 2024).
40. Solid Carbide End Mills for All Dental CNC Milling Machines and Materials. Available online: http://www.datron.co.in/brouchers/DATRON_Dental_Toolflyer_Prosp_EN.pdf (accessed on 24 June 2024).
41. Alsafi, M.S.; Abed, I.J. Effect of milling parameters on surface characteristics and mechanical properties of presintered zirconia ceramic. *Rev. Des Compos. Et Des Matériaux Avancés-J. Compos. Adv. Mater.* **2023**, *33*, 243–252. [CrossRef]
42. Walia, T.; Brigi, C.; KhirAllah, A.R.M.M. Comparative evaluation of surface roughness of posterior primary zirconia crowns. *Eur. Arch. Paediatr. Dent.* **2019**, *20*, 33–40. [CrossRef] [PubMed]
43. Wallum, A.J.; Raimondi, C.; Lien, W.; Hoopes, W.L.; Vandewalle, K.S. Effect of Milling Speed on the Properties of Zirconia Restorations. *J. Clin. Exp. Dent.* **2024**, *16*, e84. [CrossRef] [PubMed]
44. Mei, L.; Guan, G. Profilometry and atomic force microscopy for surface characterization. *Nano TransMed* **2023**, *2*, e9130017. [CrossRef]
45. Guan, G.; He, Y.; Mei, L. Atomic force microscopy: A nanobiotechnology for cellular research. *Nano TransMed* **2022**, *1*, e9130004. [CrossRef]
46. Guo, T.; Ivanovski, S.; Gulati, K. Tuning electrolyte aging in titanium anodization to fabricate nano-engineered implants. *Surf. Coat. Technol.* **2022**, *447*, 128819. [CrossRef]